

TURBULENCE IN SIMULATIONS OF BLOOD FLOW IN CEREBRAL ARTERIES WITH ANEURYSMS

Rafaello D. Luciano

Department of Mechanical Engineering
University of Saskatchewan
57 Campus Drive, Saskatoon,
SK S7N 5A9, Canada
rafaello.luciano@usask.ca

Xiongbiao Chen

Department of Biomedical Engineering
Department of Mechanical Engineering
University of Saskatchewan
57 Campus Drive, Saskatoon,
SK S7N 5A9, Canada
xbc719@mail.usask.ca

Donald J. Bergstrom

Department of Mechanical Engineering
University of Saskatchewan
57 Campus Drive, Saskatoon, SK S7N 5A9, Canada
don.bergstrom@usask.ca

ABSTRACT

In recent years, the number of studies using computational fluid dynamics to numerically simulate blood flow in arteries with aneurysms has been increasing dramatically. Although turbulent-like localized flow instabilities have been observed in studies on patients and laboratory measurements, these instabilities were rarely reported in studies involving numerical simulations. These instabilities can be important for the pathophysiology of aneurysms. Our understanding of what is required to correctly simulate these flow instabilities is still rudimentary. The present study therefore investigates OpenFOAM simulations of a realistic intracranial aneurysm geometry, looking to better understand the flow and verify the requirements, in terms of grid resolution, boundary conditions and perturbations, for reproducing these flow instabilities. The results reinforce that the outcomes of numerical simulations are very sensitive to the user set-up. The assumption by researchers that the flow is laminar is misleading, leading to the usage of methodologies that will not adequately capture the turbulence that may be present despite the very low flow rates. In addition, using fine grids with small timesteps is not sufficient to adequately capture and evaluate turbulence. Finally, the results provide further evidence that turbulence may be more prevalent in cerebral blood flow than anticipated.

INTRODUCTION

The review of Ku (1997) discussed how there is turbulence in artery stenoses around a Reynolds number of only 300, with the pulsatility of blood flow creating a periodic transition between laminar flow and turbulence. Additionally, aneurysm bruits, which are characteristic sound frequencies observed in patients with aneurysms, were associated in the past to turbulence with the explanation that an aneurysm may act as a Helmholtz resonator (Olinger and Wasserman, 1977). Several studies with patients that had intracranial aneurysms or using aneurysm glass models (Ferguson, 1972) provided sup-

porting evidence of aneurysm bruits and turbulence through experimental means. Appropriately evaluating temporal phenomena and turbulence is expected to be of importance to understanding the mechanobiology of aneurysm growth and rupture. Studies have discussed how accurate temporal wall shear-stress gradients (White et al., 2005) and turbulence (Davies et al., 1986) are important in the mechanobiology of endothelial cells, which line the interior of blood vessels.

Conversely, reports of instabilities are relatively rare in the aneurysm numerical simulation literature. This can be explained by the expectation that flow will be laminar due to the low flow rates, and the common usage of simulation setups that would be incapable of appropriately capturing and evaluating such instabilities. For example, Valen-Sendstad et al. (2014) discussed how different solver numerical settings influenced the observation of flow instabilities in aneurysms. The authors point out that the typical expectation of laminar flow in the literature is self-fulfilling, as overlooking the possibility of flow instabilities may lead to the usage of schemes and methods that render the simulations incapable of detecting said flow instabilities. However, the authors did not discuss what is necessary for the flow instabilities to appear in these simulations, nor discuss possible sources of numerical error or disturbance and how they would relate to the flow instabilities observed.

Pipes are the classical engineering geometry most related to that of arteries, and several studies, including the review of Eckhardt et al. (2007), lead to the understanding that unless a numerical simulation is perturbed enough, it will not develop from the laminar state into a turbulent one.

However, there are various other studies and examples of simulations in other fields where authors observe turbulence arising seemingly naturally, with no clear boundary or initial condition as the source of perturbation. This leads to the question of what the sources of perturbation triggering these turbulence-like flow features in cerebral aneurysm simulations are, and what is necessary in order to observe turbulence in these simulations.

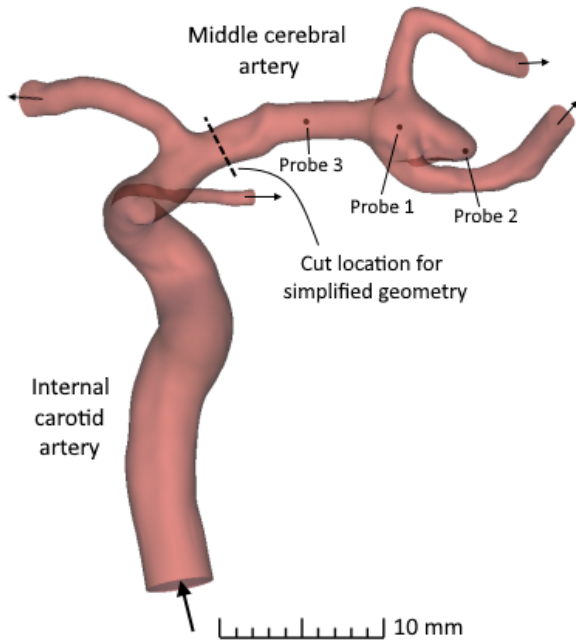


Figure 1. Artery with aneurysm geometry, with dashed line indicating the location where it was cut for the simplified geometry.

This study investigates blood flow in a realistic artery with a cerebral aneurysm, looking to evaluate the existence of turbulence, and the impact of numerical settings and perturbations on the results. Grid, cycle and phase convergence will be evaluated, in addition to looking at artificially-added perturbations to the inlet boundary condition, geometry simplifications, turbulence intensities and the turbulence energy spectra.

NUMERICAL MODEL AND METHODS

The direct numerical simulation approach was used for the transient simulations with OpenFOAM 7, using second-order accurate differencing for the spatial and temporal derivatives, with the same numerical setup that we used in our previous study (Luciano et al., 2022) with pipes at higher Reynolds numbers. Similar approaches are widely used in the literature and its quality is additionally documented, for example, in Komen et al. (2017).

The computational grids or meshes used were composed of a hexahedral core with polyhedral elements to complete it, built using ANSYS Fluent v194. Grids used in this study ranged from 200 thousand cells in the coarsest grid to 1.5 million in the finest grid, and grid dependency will be discussed in the results and limitations sections. All the results shown used the finest grid, unless otherwise specified.

The realistic geometry used for the simulations is from a 28 year old female patient and can be seen in Figure 1. This patient has a brain aneurysm in the first middle cerebral artery bifurcation. This geometry was obtained from the Aneurisk database, ecm2.mathcs.emory.edu/aneuriskweb, Case 78, database which is maintained by the Departments of Mathematics and Computer Science from Emory University, with further information available in (Sangalli et al., 2014). This specific case was chosen because there already are reports of significant flow instabilities with this geometry (Natarajan et al., 2020). The probes shown in the figure, which were used for evaluation of the simulations results,

are located along the artery and aneurysm centerlines.

The inlet boundary condition that is used for the transient simulations is the time-dependent Womersley velocity profile, which comes from the theoretical solution for laminar pulsatile flow in a straight pipe. The pulsatile flow rate used was obtained using data from real older adult patients (Hoi et al., 2010), with a cardiac cycle period of $T = 0.948$ seconds. The inlet Reynolds number for the simulations ranged from 211 to 627 throughout the cardiac cycle, with an average of 379. For the simulations that used the simplified geometry, which discarded the internal carotid artery (ICA) with the inlet then positioned at the beginning of the middle cerebral artery (MCA), see Figure 1, the inlet flow rate was estimated using a flow rate splitting method based on the physiological Murray law and described in Chnafa et al. (2018). A pulsatility dampening factor was also applied on the inlet flow waveform to account for the reduction in pulsatility observed in patients from the ICA to the MCA. A pulsatility reduction or dampening of 7.4% was therefore considered for the simplified geometry with the inlet at the MCA, based on the research of Zarrinkoob et al. (2016) with elderly patients.

A steady-state laminar simulation was also used for comparison purposes, and it had a Hagen-Poiseuille profile specified at the inlet, with the flow rate equivalent to the averaged Reynolds number in the pulsatile simulation. The numerical setup of this simulation was also more dissipative in order to suppress the turbulence and obtain a laminar solution.

The no-slip boundary condition is used at the walls, and the artery walls were assumed to be rigid. Wall compliance is considered to be of relatively low importance in cerebral blood flow, not to mention the associated uncertainties and significantly increased computational costs (Steinman and Pereira, 2019). Similarly, modeling blood as a non-Newtonian fluid is also considered to be of less importance and associated with significant uncertainties, so in this study blood is represented as a Newtonian fluid with kinematic viscosity of 3.5 cP and density of 1060 kg/m³. Lastly, the outlet boundary conditions for the transient pulsatile simulations were estimated using the already mentioned flow rate splitting method based on the Murray law (Chnafa et al., 2018).

The unrealistic initial condition that is given to the simulation significantly perturbs the initial simulation time steps. After around one fifth to one fourth of the first cardiac cycle had been simulated these initial transients were mostly washed out and not as noticeable. It is relevant to note that the fluid residence time within these arteries is significantly shorter than a cardiac cycle. The longest artery simulated has an estimated maximum residence time, from the inlet to the furthest outlet, of less than half a cardiac cycle. Due to the initial perturbation, we observed that discarding the first simulated cardiac cycle made a noticeable difference in the energy spectra and turbulence intensity results. Discarding more than one cardiac cycle did not make as significant of a difference, particularly considering the uncertainty due to the reduced number of cardiac cycles being taken into account when discarding more initial cycles. Nonetheless, for this paper we discarded the first two initial cycles of a total of 30 simulated, and present the results based on the remaining 28 cardiac cycles.

RESULTS AND DISCUSSION

Figure 2 shows the results on different grids for the volume-averaged turbulence intensity within the region near the aneurysm. These grid convergence results are based on simulations with 28 cardiac cycles averaged and data sampled

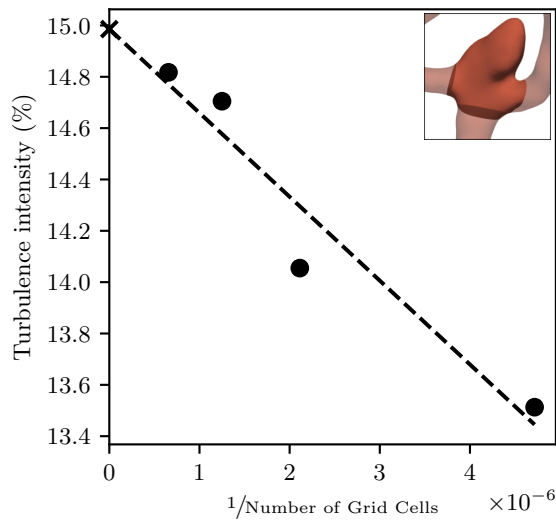


Figure 2. Grid convergence results for volume-averaged turbulence intensity. The region for volume-averaging is the one highlighted with no transparency in the geometry view at the top right corner.

at a frequency of 20 phases per period (or 20 times per cardiac cycle), with more discussion about these values in the limitations section. With the grid convergence index (GCI) method of Roache (1997), which is based on the generalized Richardson extrapolation, using the 2 finest grids and the coarsest one, a relative uncertainty of the turbulence intensity for the finest grid around 0.5% was estimated. A linear fit (shown in the figure) through all the grid results and extrapolated to what would be the grid with an infinite number of cells, results in a relative difference around 1% for the finest grid compared to the extrapolated one.

One behavior that is noticeable in Figure 2 and that was not expected is the fact that using finer grids is producing simulations that have higher turbulence intensities. This is opposite to the behavior observed in our previous study with pipes and somewhat higher Reynolds numbers (Luciano et al., 2022), where more refined grids were observed to produce less turbulent, even laminar, simulations compared to coarser grids that were more turbulent. We believe this behavior in the previous study was due to the increase of numerical discretization errors by using coarser grids, which perturbed the simulation.

In the present aneurysm simulations which are at very low Reynolds numbers, it seems that the additional perturbations introduced when using coarser grids are not enough to counteract the spatial resolution that is lost, with the resulting turbulence intensity being reduced. Another, more likely, possibility is that the aneurysm simulation was already perturbed enough by numerical noise, even in the finest grids. Therefore, additional perturbation from using coarser grids did not make a difference, as a perturbation threshold was reached and crossed with additional perturbations not significantly influencing the turbulent behavior. This behavior with the existence of a maximum perturbation threshold, and additional perturbations over the threshold not making a difference, was also seen in the previous study mentioned. Lastly, this also shows how sensitive the cerebral aneurysm simulations are to perturbations and noise.

When evaluating the convergence of the turbulence intensity calculation considering the number of phases per period being sampled and averaged, i.e. how many times data is sam-

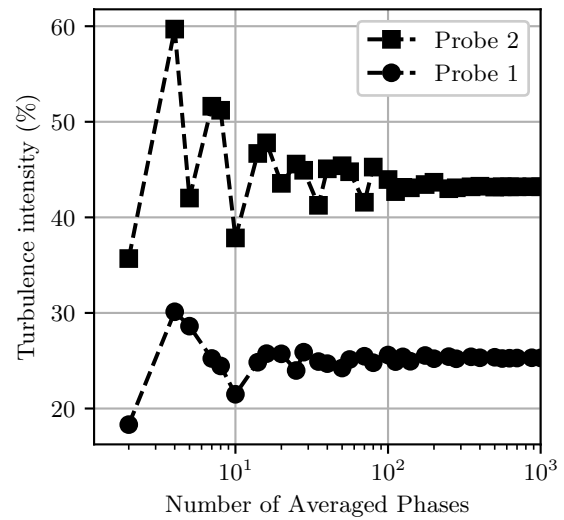


Figure 3. Phase convergence of the turbulence intensity results.

pled per cardiac cycle, the results obtained are seen in Figure 3. For this evaluation, the raw data was sampled at specified points (see the probes in Figure 1) at solver resolution with a sampling frequency of about 74 kHz, or 70,000 time steps per cardiac cycle, for the 28 cardiac cycles averaged. The raw probe data was then “sampled” at different frequencies, using factor frequency numbers with no interpolation, to simulate as accurately as we can what would happen if the actual simulation data had been sampled at a lower frequency. The data for probe 3 is not shown in this plot because the results for turbulence intensity are 0% (around 10^{-6}) regardless of the number of averaged phases, due to flow being laminar in the region around probe 3.

There is a clear convergence of the turbulence intensity results when the number of phases being averaged increases, with about 1,000 phases producing turbulence intensity results for probes 1 and 2 within 0.01%, relative, of the converged value and 10,000 phases with relative differences on the order of 10^{-8} . For the results further from convergence, with around 20 phases, they are varying roughly within 10% of the converged value (e.g. for probe 2, $43.2 \pm 4.3\%$), and with 100 phases within 2% ($43.2 \pm 0.9\%$).

Now evaluating the influence of the number of cardiac cycles being averaged, from 2 to 28, using the data sampled at solver frequency, the results are shown in Figure 4. A linear fit of the results is also displayed in this figure. The number of cycles being averaged makes a significant difference in the turbulence intensity results compared to the linearly extrapolated value, with relative differences of 10% up to around 15 cycles and around 2% for 28 cycles.

The averaged energy spectrum periodogram, using the full probe data at 70,000 phases per cardiac cycle (74 kHz) with the finest grid, for the velocity fluctuation component in the x-direction, is shown in Figure 5. The x-direction is aligned with the inlet flow direction, but the three velocity fluctuation components had the same behavior so only one of them is shown here. The energy spectrum was averaged using the Bartlett method with 1000 non-overlapping segments in order to reduce the variance and facilitate the observation of the overall trend of the data. The energy is normalized by dividing it by the bulk velocity at the inlet squared, and the frequency is normalized by multiplying it by the cardiac cycle period.

It is surprising to notice that, despite the very low

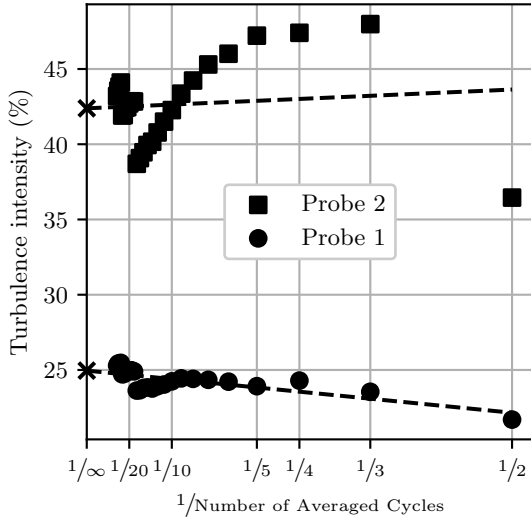


Figure 4. Cycle convergence of the turbulence intensity results.

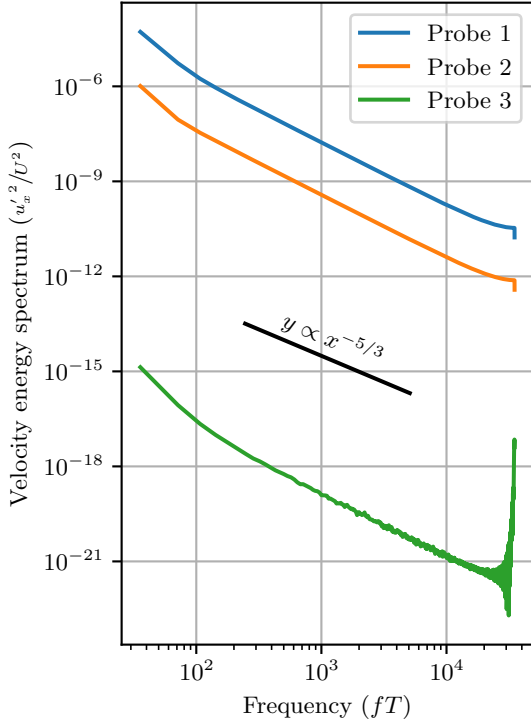


Figure 5. Averaged energy spectrum of the velocity fluctuations.

Reynolds numbers and no attempt being made to identify the inertial range, the averaged roll-off of the velocity energy spectrum at all probes is only slightly faster (exponent more negative) than the Kolmogorov $-\frac{5}{3}$ spectrum. Saqr et al. (2020) observed much faster roll-offs in intracranial aneurysms in theoretical calculations and patient measurements, however they only looked at frequencies up to 50 Hz.

In addition, there is the evidence of an inverse energy cascade at the highest frequencies for probe 3 in Figure 5. As probe 3 is located in a region where the flow is laminar, we believe this inverse energy cascade may be simply due to numerical error as these frequencies are approaching the solver time stepping resolution. This may also be related to how infinitesimal numerical errors or noise can influence the simulation and

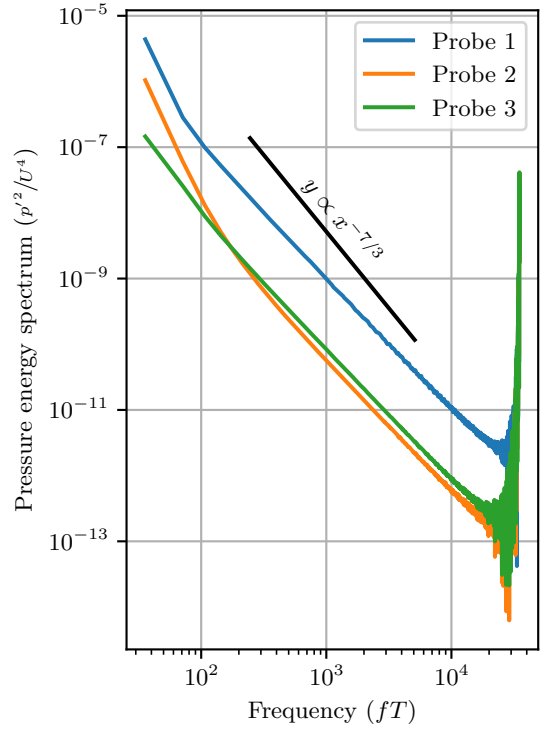


Figure 6. Averaged energy spectrum of the pressure fluctuations.

cause turbulence regardless of the existence of other sources of perturbations, through the introduction of energy at solver resolution. Saqr et al. (2022) also observed a significant inverse energy cascade, though at much lower frequencies than the ones being evaluated in the present paper.

The averaged energy spectrum of the pressure fluctuations, Figure 6, is also surprisingly close but conversely has a slightly slower roll-off than the $-\frac{7}{3}$ exponent that would be expected for high Reynolds number flows and high frequencies (George et al., 1984). Also noticeable is the previously mentioned inverse energy cascade at the highest frequencies, but now in all three probes.

Two additional topics were evaluated: (i) the addition of random normally-distributed perturbations with intensity equivalent to 5% turbulence intensity superimposed on the Womersley inlet velocity boundary condition, similar to the perturbations previously used in Luciano et al. (2022), and (ii) the simplification of the geometry by cutting off the upstream arteries from the aneurysm down to the middle cerebral artery, as schematized by the cutting line in Figure 1. Both were evaluated through the volume-averaged turbulence intensity within the aneurysm (see Figure 2), with the resolution of the finest grid and with 100 phases being sampled per cycle.

Regarding (i), when adding random perturbations to the inlet there was no significant difference in the aneurysm turbulence intensity results, with the relative difference on the order of 10^{-4} . This shows that the inlet in the full geometry is far away enough that these perturbations have the time to dissipate before reaching the aneurysm, therefore not significantly influencing the turbulence intensity inside the aneurysm. This behavior may have been different if all sources of numerical noise were sufficiently reduced, and the only source of perturbation was the perturbation at the inlet. In this case, we expect the added perturbation would be necessary in order to trigger turbulence in this flow.

As for (ii), the simplification of the geometry by cutting

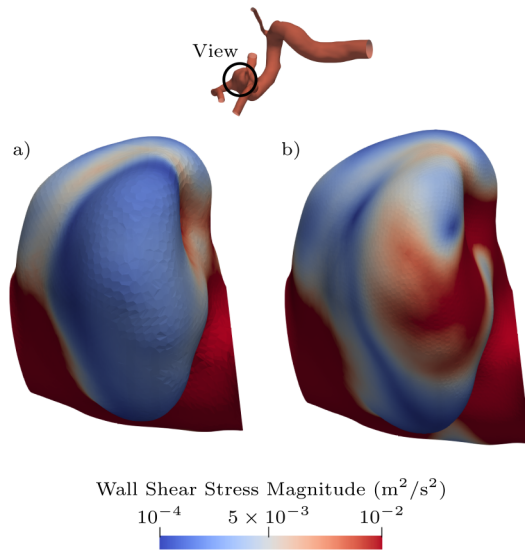


Figure 7. Comparison of wall shear stress magnitude results for (a) steady-state laminar simulation and (b) time-averaged turbulent simulation.

it at the beginning of the MCA does make a significant difference by relatively increasing the turbulence intensity within the aneurysm by more than 10%. This is despite the fact that dampening was added to the flow rate waveform of the MCA inlet in the simulation with the cut geometry.

The results of the steady-state laminar simulation are compared to the turbulent simulation in Figure 7. The steady-state laminar and transient turbulent aneurysm wall shear stress magnitude results are completely different. The turbulent results show averaged wall shear stress values that are about 5 times higher than the laminar solution around the center of the aneurysm wall in the figure, and this is based on the time-average and not the transient peaks which will be even higher in the turbulent simulation. Needless to say, the assumption that flow is laminar is completely misleading. In fact, as shown in the previous images (figures 2-4), turbulence intensity values approaching 50% are observed, and when volume-averaged through the entire aneurysm region are around 15% indicating a highly turbulent flow.

Limitations

Several limitations had to be imposed on the simulations and post-processing in order to enable the feasibility of this study in the time-frame available, limitations which will affect the results to varying degrees.

The grid dependency evaluation is planned to be redone based on the aggregate results obtained from this study, with additional grids. Even though the general trend may have been captured correctly, increasing the number of phases, i.e. sampling frequency, was shown to be important (see Figure 3). Only 20 phases were used for the preliminary grid evaluation discussed here, which means that the different grid results are almost within each others' uncertainties. Note that this grid evaluation was the first step in the present study. Ideally, at least 100 phases should be used due to the associated uncertainties observed (even better using probes at solver time step resolution as done for other simulations in the present study), also with significantly more than 30 averaged cardiac cycles, to limit the propagation of uncertainties. For reference, An-

dersson and Karlsson (2021) have evaluated up to 80 cardiac cycles with 100 phases.

Related to the previous point, additional cardiac cycles to the 30 we simulated for this paper would be important not only in order to better evaluate the number of cycles required for an acceptable solution, but also to provide additional data on whether discarding more than two of the initial cardiac cycles is beneficial at all. This could be done while using probes sampling data at solver time step frequency in order to eliminate any concerns with the sampling frequency.

The time step dependence (i.e. the temporal convergence) of the results was also not evaluated in detail. We maintained the time step sizes low enough so that the Courant-Friedrich-Lewy (CFL) number was always lower than 1, which resulted in the time step frequency of 70,000 times per cardiac cycle. We did not evaluate whether lowering them even further or raising them above $CFL = 1$ made any difference in the results. With that said, the time step sizes should definitely be significantly smaller than the equivalent to 100 time steps per cycle as that would be close to the least required for an acceptable phase-average, never mind the temporal resolution of the simulation itself. For reference, the results in Luciano et al. (2022) show that time steps as low as $CFL = 0.1$ could potentially make a difference in the results of relatively low Reynolds number simulations.

Lastly, the turbulence intensity was the main output variable evaluated in this study. Simultaneously evaluating other variables such as the wall shear stress could be useful particularly towards clinical practice, though that leads into other uncertainties and discussions such as what hemodynamics variables are actually important for the pathophysiology of this vascular disease.

CONCLUSIONS

Not only is there turbulence in the artery with an aneurysm simulated here, this is in reality a highly turbulent flow, despite the very low Reynolds numbers involved.

The common assumptions in the literature that blood flow is laminar and that the evaluation of a few cardiac cycles is enough are misleading. Appropriately capturing the very complex turbulence in the flow could be very important for physicians and researchers. In addition, in order to save computational costs, researchers often set the inlet of the computational artery geometry close to where the aneurysm is, but our simulations show that this simplification can also make a significant difference in the turbulence intensity within the aneurysm.

As general recommendations for the simulation of cerebral aneurysms, based on this study as lower bounds it would be suggested that (i) at least 30 cardiac cycles are simulated while discarding the first cycle due to initial transients, (ii) data is sampled at least 100 times per cardiac cycle for phase-averaging and (iii) as much of the real geometry is used as feasible. Lastly, all of these should be evaluated on a case-by-case basis, as we believe the requirements may vary significantly and it is always important to be aware of the associated uncertainties.

REFERENCES

- Andersson, M. and Karlsson, M. 2021 Model Verification and Error Sensitivity of Turbulence-Related Tensor Characteristics in Pulsatile Blood Flow Simulations. *Fluids* **6**(1) 11.
Chnafa, C., Brina, O., Pereira, V. M. and Steinman, D. A. 2018 Better Than Nothing: A Rational Approach for Minimizing

- the Impact of Outflow Strategy on Cerebrovascular Simulations. *American Journal of Neuroradiology* **39**(2) 337–343.
- Davies, P. F., Remuzzi, A., Gordon, E. J., Dewey, C. F. and Gimbrone, M. A. 1986 Turbulent fluid shear stress induces vascular endothelial cell turnover in vitro. *Proceedings of the National Academy of Sciences of the United States of America* **83**(7) 2114–2117.
- Eckhardt, B., Schneider, T. M., Hof, B. and Westerweel, J. 2007 Turbulence Transition in Pipe Flow. *Annual Review of Fluid Mechanics* **39**(1) 447–468.
- Ferguson, G. G. 1972 Physical factors in the initiation, growth, and rupture of human intracranial saccular aneurysms. *Journal of Neurosurgery* **37**(6) 666–677.
- George, W. K., Beuther, P. D. and Arndt, R. E. A. 1984 Pressure spectra in turbulent free shear flows. *Journal of Fluid Mechanics* **148** 155–191.
- Hoi, Y., Wasserman, B. A., Xie, Y. J., Najjar, S. S., Ferruci, L., Lakatta, E. G., Gerstenblith, G. and Steinman, D. A. 2010 Characterization of volumetric flow rate waveforms at the carotid bifurcations of older adults. *Physiological Measurement* **31**(3) 291–302.
- Komen, E. M. J., Camilo, L. H., Shams, A., Geurts, B. J. and Koren, B. 2017 A quantification method for numerical dissipation in quasi-DNS and under-resolved DNS, and effects of numerical dissipation in quasi-DNS and under-resolved DNS of turbulent channel flows. *Journal of Computational Physics* **345** 565–595.
- Ku, D. N. 1997 Blood Flow in Arteries. *Annual Review of Fluid Mechanics* **29**(1) 399–434.
- Luciano, R. D., Chen, X. B. and Bergstrom, D. J. 2022 Discretization and perturbations in the simulation of localized turbulence in a pipe with a sudden expansion. *Journal of Fluid Mechanics* **935** A20.
- Natarajan, T., MacDonald, D. E., Najafi, M., Coppin, P. W. and Steinman, D. A. 2020 Spectral decomposition and illustration-inspired visualisation of highly disturbed cerebrovascular blood flow dynamics. *Computer Methods in Biomechanics and Biomedical Engineering: Imaging & Visualization* **8**(2) 182–193.
- Olinger, C. P. and Wasserman, J. F. 1977 Electronic stethoscope for detection of cerebral aneurysm, vasospasm and arterial disease. *Surgical Neurology* **8**(4) 298–312.
- Roache, P. J. 1997 Quantification of uncertainty in computational fluid dynamics. *Annual Review of Fluid Mechanics* **29**(1) 123–160.
- Sangalli, L. M., Secchi, P. and Vantini, S. 2014 AneuRisk65: A dataset of three-dimensional cerebral vascular geometries. *Electronic Journal of Statistics* **8**(2) 1879–1890.
- Saqr, K. M., Tupin, S., Rashad, S., Endo, T., Niizuma, K., Tominaga, T. and Ohta, M. 2020 Physiologic blood flow is turbulent. *Scientific Reports* **10**(1) 15492.
- Saqr, K. M., Kano, K., Rashad, S., Niizuma, K., Kaku, Y., Iwama, T. and Tominaga, T. 2022 Non-Kolmogorov turbulence in carotid artery stenosis and the impact of carotid stenting on near-wall turbulence. *AIP Advances* **12**(1) 015124.
- Steinman, D. A. and Pereira, V. M. 2019 How patient specific are patient-specific computational models of cerebral aneurysms? An overview of sources of error and variability. *Neurosurgical Focus* **47**(1) E14.
- Valen-Sendstad, K., Piccinelli, M. and Steinman, D. A. 2014 High-resolution computational fluid dynamics detects flow instabilities in the carotid siphon: Implications for aneurysm initiation and rupture? *Journal of Biomechanics* **47**(12) 3210–3216.
- White, C. R., Stevens, H. Y., Haidekker, M. and Frangos, J. A. 2005 Temporal gradients in shear, but not spatial gradients, stimulate ERK1/2 activation in human endothelial cells. *American Journal of Physiology-Heart and Circulatory Physiology* **289**(6) H2350–H2355.
- Zarrinkoob, L., Ambarki, K., Wählin, A., Birgander, R., Carlberg, B., Eklund, A. and Malm, J. 2016 Aging alters the dampening of pulsatile blood flow in cerebral arteries. *Journal of Cerebral Blood Flow & Metabolism* **36**(9) 1519–1527.